Multistatic Measurements in a Controlled Laboratory Environment

Ivan Bradaric[*], Gerard T. Capraro[*], Steven H. Brady[+], Michael A. Saville[+] and Michael C. Wicks[^]

[*] Capraro Technologies, Inc., Utica, NY, USA

[+] Department of Electrical and Computer Engineering, Air Force Institute of Technology, Wright-Patterson AFB, OH, USA

[^] U. S. Air Force Research Laboratory, Sensors Directorate, USA

***Abstract*— In recent years, a novel mathematical framework for analyzing and designing multistatic radar systems has been proposed. It was argued through numerous simulation examples that multistatic radar system performances can be significantly improved by shaping the multistatic ambiguity function. Based on this framework, rules for waveform selection, sensor positioning and adequate weighting of different receivers have been developed. In this work, we present multistatic measurements obtained in a controlled laboratory environment to support some of these recent findings and conclusions. The experimental setup consists of a Lab-Volt™ radar system operating at X-band, Tektronix arbitrary waveform generator and Tektronix digital oscilloscope. Multistatic point target radar measurements for different system configurations are analyzed.**

I. Introduction

The ambiguity function is a widely used tool for the analysis of radar systems. In recent years there have been considerable efforts to formulate the ambiguity function for bistatic and multistatic radar systems. In [1], the authors developed the ambiguity function for bistatic radar systems. This work was extended in [2] to the case of multistatic radar systems. In [3-6], the multistatic ambiguity function was used for assessing waveform selection, sensor positioning and coherent signal processing strategies. It was demonstrated through simulations that multistatic radar system performances can be improved by adequately shaping the multistatic ambiguity function.

In this work, we try to substantiate some of the findings and conclusions presented in the above mentioned papers. To accomplish this goal we collect and analyze multistatic measurements obtained in a controlled laboratory environment. The experimental setup is designed to replicate the system assumptions made in the previous simulations. The paper is organized as follows. In Section II, we briefly outline the basic mathematical concepts behind the multistatic ambiguity function. In Section III we review some simulation examples used to illustrate the significance of the multistatic ambiguity function. Experimental setup used for collecting the multistatic measurements is described in Section IV. In Section V, we analyze the obtained measurements and investigate how they relate to the simulation results. Finally, in Section VI we provide concluding remarks.

II. Multistatic Ambiguity Function

We consider a single transmitter multiple receiver radar system and assume that a coherent processing interval consists of a single pulse $s(t)$ given as:

$$s(t) = \sqrt{2E}\,\mathrm{Re}\left\{ \tilde{f}(t) e^{j\omega_c t} \right\} \quad , \quad 0 \le t \le T_d \tag{1}$$

where $\mathrm{Re}\{\cdot\}$ denotes the real part operator, $\tilde{f}(t)$ is the complex envelope of the transmitted pulse, E and T_d are the energy and duration of the pulse, respectively, and $\omega_c = 2\pi f_c$ is the carrier frequency.

Let the complex envelope of the i^{th} receiver input $(i = 1, 2, ..., N)$ be denoted by $\tilde{r}_i(t)$. According to whether a target is absent (H_o) or present (H_1), the two hypotheses are presented as

$$\begin{aligned} H_0 &: \tilde{r}_i(t) = \tilde{n}_i(t) \\ H_1 &: \tilde{r}_i(t) = \tilde{a}_i \tilde{s}(t - \tau_{ai}) e^{j\omega_{Dai} t} + \tilde{n}_i(t) \end{aligned} \tag{2}$$

where $\tilde{a}_i$ is a complex gain which accounts for propagation and scattering effects along the i^{th} path between the transmitter, target and the i^{th} receiver. τ_{ai} and ω_{Dai} denote the actual total delay and Doppler shift experienced by the transmitted signal along the i^{th} path, and $\tilde{n}_i(t)$ denotes the complex envelope of the additive noise present at the i^{th} receiver input.

Assuming additionally that the envelopes $\tilde{n}_i(t)$ are complex Gaussian random processes with zero-mean and white in quadrature components with power spectral densities $N_{0i}/2$, the signal at the output of the matched filter of the i^{th} receiver becomes

Report Documentation Page

Form Approved
OMB No. 0704-0188

1. REPORT DATE	2. REPORT TYPE	3. DATES COVERED
MAY 2010		**00-00-2010 to 00-00-2010**

4. TITLE AND SUBTITLE	5a. CONTRACT NUMBER
Multistatic Measurements in a Controlled Laboratory Environment	5b. GRANT NUMBER
	5c. PROGRAM ELEMENT NUMBER
6. AUTHOR(S)	5d. PROJECT NUMBER
	5e. TASK NUMBER
	5f. WORK UNIT NUMBER
7. PERFORMING ORGANIZATION NAME(S) AND ADDRESS(ES) **Air Force Institute of Technology,Department of Electrical and Computer Engineering,Wright-Patterson AFB,OH,45433**	8. PERFORMING ORGANIZATION REPORT NUMBER
9. SPONSORING/MONITORING AGENCY NAME(S) AND ADDRESS(ES)	10. SPONSOR/MONITOR'S ACRONYM(S)
	11. SPONSOR/MONITOR'S REPORT NUMBER(S)

12. DISTRIBUTION/AVAILABILITY STATEMENT
Approved for public release; distribution unlimited

13. SUPPLEMENTARY NOTES
See also ADM002322. Presented at the 2010 IEEE International Radar Conference (9th) Held in Arlington, Virginia on 10-14 May 2010. Sponsored in part by the Navy.

14. ABSTRACT
In recent years, a novel mathematical framework for analyzing and designing multistatic radar systems has been proposed. It was argued through numerous simulation examples that multistatic radar system performances can be significantly improved by shaping the multistatic ambiguity function. Based on this framework, rules for waveform selection, sensor positioning and adequate weighting of different receivers have been developed. In this work, we present multistatic measurements obtained in a controlled laboratory environment to support some of these recent findings and conclusions. The experimental setup consists of a Lab-VoltTM radar system operating at X-band, Tektronix arbitrary waveform generator and Tektronix digital oscilloscope. Multistatic point target radar measurements for different system configurations are analyzed.

15. SUBJECT TERMS

16. SECURITY CLASSIFICATION OF:			17. LIMITATION OF ABSTRACT	18. NUMBER OF PAGES	19a. NAME OF RESPONSIBLE PERSON
a. REPORT **unclassified**	b. ABSTRACT **unclassified**	c. THIS PAGE **unclassified**	**Same as Report (SAR)**	**5**	

$$d_i = \left| \int_{-\infty}^{\infty} \frac{\tilde{r}_i(t)}{\sqrt{N_{0i}}} \tilde{f}^*(t-\tau_{Hi}) e^{-j\omega_{DHi}t} dt \right| \quad (3)$$

where $\tilde{f}^*(t)$ denotes complex conjugate of $\tilde{f}(t)$, and τ_{Hi} and ω_{DHi} denote the hypothetical total delay and Doppler shift experienced by the transmitted signal assuming a target present in the radar cell under test.

Signals d_i, $i = 1, 2, ..., N$, represent local statistics obtained at each receiver. The ambiguity function for the i^{th} receiver becomes [2]

$$\Theta_i(\tau_{Hi}, \tau_{ai}, \omega_{DHi}, \omega_{Dai}) = \left| \int_{-\infty}^{\infty} \tilde{f}(t-\tau_{ai}) \tilde{f}^*(t-\tau_{Hi}) e^{j(\omega_{Dai}-\omega_{DHi})t} dt \right|^2. \quad (4)$$

The global ambiguity function is then given as a weighted sum of the bistatic ambiguity functions:

$$\Theta(\boldsymbol{\tau}_H, \boldsymbol{\tau}_a, \boldsymbol{\omega}_{DH}, \boldsymbol{\omega}_{Da}) = \sum_{i=1}^{N} c_i \Theta_i(\tau_{Hi}, \tau_{ai}, \omega_{DHi}, \omega_{Dai}) \quad (5)$$

where

$$\boldsymbol{\tau}_H = [\tau_{H1}, \tau_{H2}, \ldots, \tau_{HN}]^T,$$
$$\boldsymbol{\tau}_a = [\tau_{a1}, \tau_{a2}, \ldots, \tau_{aN}]^T,$$
$$\boldsymbol{\omega}_{DH} = [\omega_{DH1}, \omega_{DH2}, \ldots, \omega_{DHN}]^T,$$
$$\boldsymbol{\omega}_{Da} = [\omega_{Da1}, \omega_{Da2}, \ldots, \omega_{DaN}]^T$$

and c_i, $i = 1, ..., N$ are the weighting coefficients that satisfy the relationship $\sum_{i=1}^{N} c_i = 1$.

The ambiguity function $\Theta(\boldsymbol{\tau}_H, \boldsymbol{\tau}_a, \boldsymbol{\omega}_{DH}, \boldsymbol{\omega}_{Da})$ for a given target (fixed $\boldsymbol{\tau}_a$ and $\boldsymbol{\omega}_{Da}$) is a $2N$- dimensional function. Since we are ultimately interested in target position (defined by its coordinates, e.g. x, y and z) and its velocity vector (defined by its components, e.g. $\dot{x}$, $\dot{y}$ and $\dot{z}$) it is more practical to express the ambiguity function as a function of these quantities. The highly nonlinear nature of mapping between the delays and Doppler shifts on one hand, and target coordinates and its velocity vector components on the other, makes the analysis of multistatic radar systems especially challenging and the system geometry very important. It should be pointed out that this nonlinearity does not exist in monostatic radar systems.

Thus, to simplify the analysis, but more importantly, to account for the system geometry when formulating the multistatic ambiguity function, we align all receivers with respect to the target position and velocity. In addition, in order to visualize the problem we usually select two fixed dimensions to present the multistatic ambiguity function. In this paper, we will consider 2-D system geometries and concentrate on target position only. Thus, the multistatic ambiguity function will be presented as a function of x and y coordinates only.

III. Simulation Results

We will now illustrate the multistatic ambiguity function using the example borrowed from [5]. Let us consider a 2-D multistatic system configuration with 4 receivers and one transmitter as shown in Figure 1.

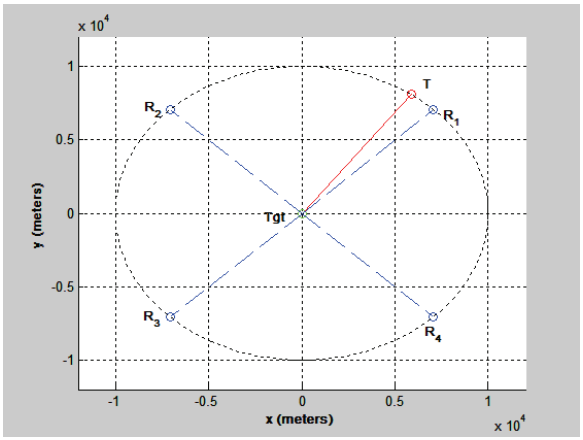

Figure 1. Multistatic system geometry

Without the loss of generality, the target is placed at the origin (labeled *Tgt*), four receivers are shown as R_i, $i = 1, 2, 3, 4$ and the transmitter is shown as T. The distance between the target and all the sensors (transmitter and receivers) is assumed to be 10 km.

Assume that we are interrogating a relatively small area (100m x 100m) as compared to distances between the sensors and that range resolution is our primary concern. In this example the transmitted waveform is a single pulse Barker 13 waveform with the pulse width of 44 ns. We will also assume that all receivers are weighted equally (a reasonable assumption since all distances are the same). The multistatic ambiguity function (presented in x-y plane) is shown in Figure 2, while the corresponding 3-dB main lobe contour plot is shown in Figure 3.

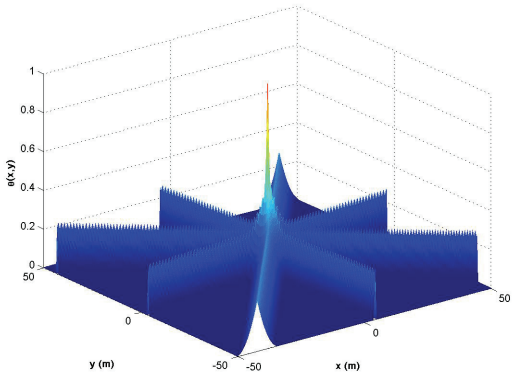

Figure 2. Multistatic ambiguity function

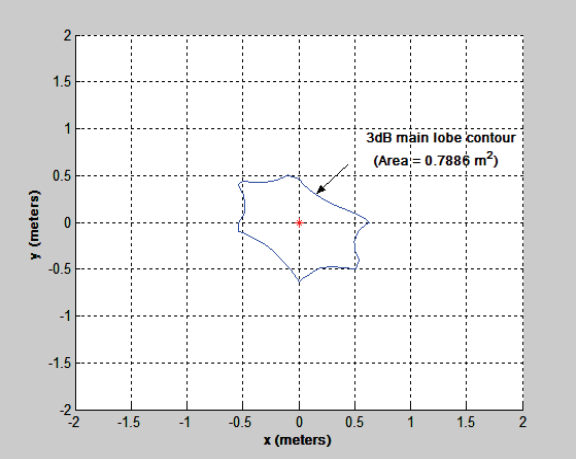

Figure 3. Multistatic ambiguity function (3-dB contour plot)

The area of the 3-dB main lobe contour in this example is 0.7886 m^2. Note that a 3-dB area of the multistatic ambiguity function is closely related to the resolution of the corresponding multistatic radar system.

Let us now consider a scenario where positions of all receivers are fixed, while the position of the transmitter can change as long as the distance from the origin remains the same (10 km). In particular, let us move the transmitter along the arc shown in Figure 4.

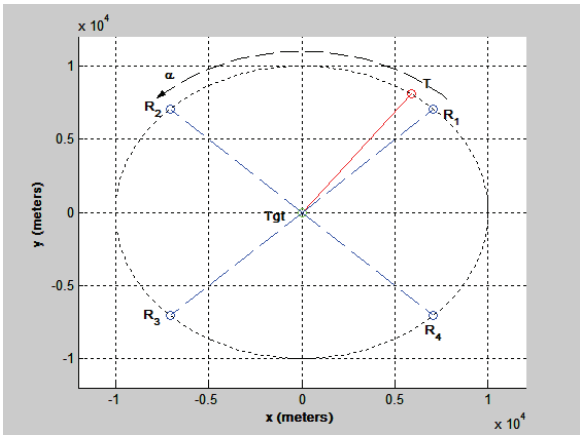

Figure 4. Multistatic system geometry (moving transmitter)

Figure 5 shows the 3-dB main lobe contour area results for different transmitter positions (angle α was varied between 0 and π/2 (see Figure 4)). As can be seen in Figure 5, in order to achieve the best range resolution, the transmitter should be placed right in the middle between receivers R_1 and R_2. As the transmitter moves closer to one of the receivers, the range resolution deteriorates (note that $\alpha = 0.05\pi$ in Figure 3). This is a somewhat expected result that we will try to verify and substantiate with real measurements.

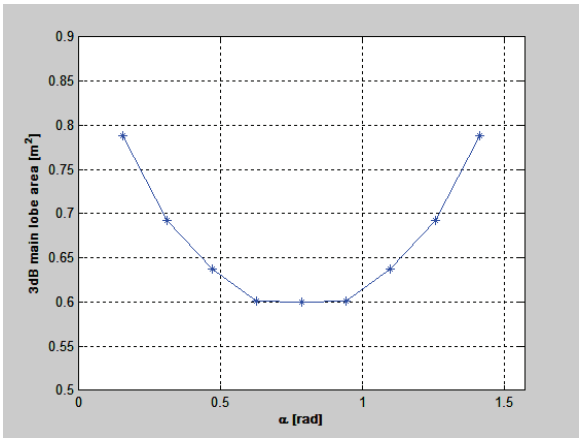

Figure 5. 3-dB main lobe area results (moving transmitter)

IV. Experimental Setup

Our measurement equipment consists of a Lab-Volt™ radar system operating at X-band, Tektronix arbitrary waveform generator (AWG) and a Tektronix digital oscilloscope. The Lab-Volt™ is described in detail in [7], and provides many of the basic components needed for timing and synchronization of the Single Input Multiple Output (SIMO) system that is of interest here. Tektronix arbitrary waveform generator creates the phase coded baseband signals, the Lab-Volt X-band source, antennas, synchronizer, and target positioner are combined with additional mixers and filters to form the radar front end, and the Tektronix digital oscilloscope serves as the digital receiver. The complete system is presented in a companion paper [8].

The high-speed sampling capability allows data capture at radio frequencies (RF) and baseband conversion is performed digitally in MATLAB. As the bistatic receiver is repositioned around the circle, the transmit waveform is rebroadcast so that subsequent measurements can be assembled as if *N* receivers were simultaneously operated. This approach essentially simulates a single transmitter multiple receiver operation and the data can be used to support various SIMO signal processing algorithms.

The measurement equipment is shown in Figure 6. To meet our goal of closely matching the simulation assumptions made in [5] the system is configured as shown in Figure 7. At the center of the circle in Fig. 7 is a point target (1-in metal sphere). The primary receiver is co-located with the transmitter in a monostatic configuration and the remaining receivers are positioned at multiple locations around the circle. As depicted in Fig. 7, the particular set up only supports two simultaneously operated receive channels. However, by keeping the transmit path and waveform exactly the same (a distinct advantage of using the AWG), we can reposition the secondary receiver and repeat the experiment to obtain *N* different receive locations. This process simulates *N* simultaneously operated receivers and serves as a way to scale the measurement for the laboratory environment that may otherwise suffer mutual coupling effects between the various receive antennas when operated in close proximity.

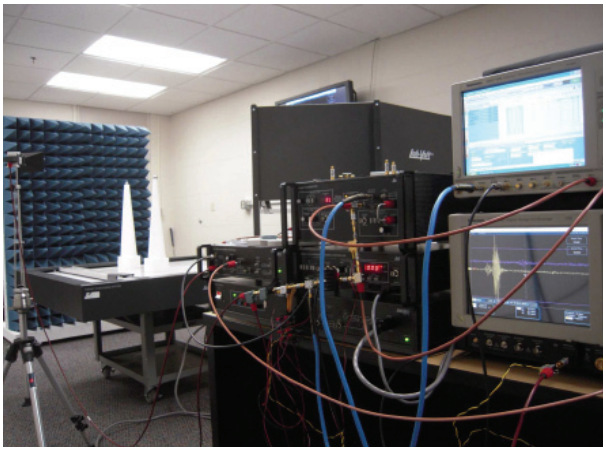

Figure 6. Measurement equipment

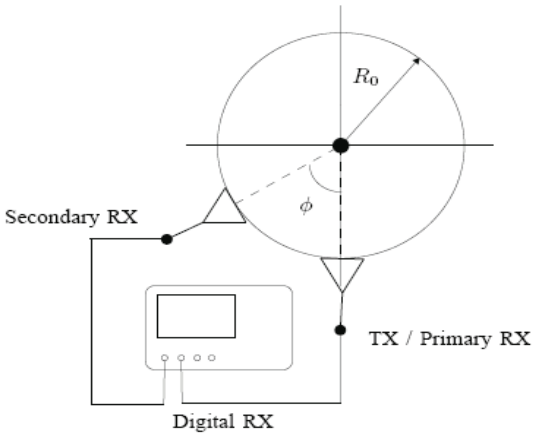

Figure 7. Laboratory setup

V. Measurement Results

Our measured data were obtained using a carrier frequency of approximately $f_c = 10$ GHz, 4-element Barker code transmitting waveform (phase sequence: 0, 0, 0, π, with 0.5 ns chip width) and measurement radius $R_o = 1.02$ m (see Fig. 7).

In order to relate our measurements with the simulation results presented in Section III let us first consider the simulated configuration with four receivers and the transmitter located at $\alpha = \pi/4$ (see Figure 4). Recall that this was the configuration that had the best resolution as measured by the 3-dB main lobe contour area. In order to create the same configuration we positioned four bistatic receivers at $\phi_1 = \pi/4$, $\phi_2 = 7\pi/4$, $\phi_3 = 5\pi/4$ and $\phi_4 = 3\pi/4$ (see Figure 7). Let us process the signal measured at the first receiver ($\phi_1 = \pi/4$) and converted to baseband. The corresponding output of the matched filter correlator is shown in Figure 8. Note that this signal represents the local statistics as defined by Eq. (3) and integrated over 100 pulses.

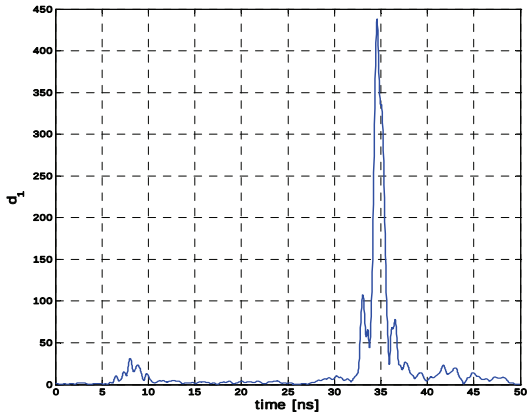

Figure 8. Output of the matched filter correlator

Similar results are obtained for the remaining three receivers. Next we align and combine the obtained results to create the corresponding data cube plots that should represent the shape of the multistatic ambiguity function. We assume that the interrogation area is a square 2m x 2m with the target placed at the origin and oriented the same way as the laboratory setup shown in Figure 7. Figure 9 shows the corresponding normalized bistatic data cube (Receiver 1) where global statistics is formed as $D = d_1^2$.

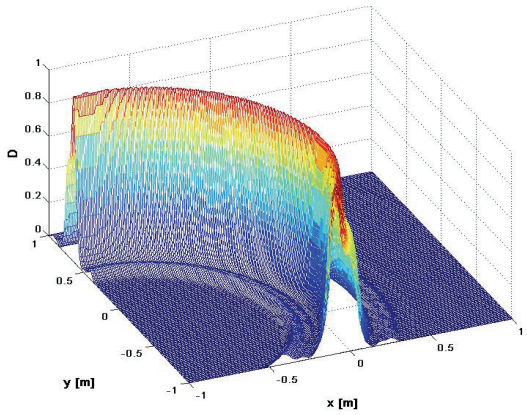

Figure 9. Normalized bistatic data cube

Figure 10 shows the corresponding normalized multistatic data cube where the global statistic is formed as:

$$D = w_1 d_1^2 + w_2 d_2^2 + w_3 d_3^2 + w_4 d_4^2 \qquad (6)$$

where w_1, w_2, w_3 and w_4 are the weights associated with each receiver.

In this example signals from all receivers are first normalized and then weighted equally. This was done in order to relate obtained measurements with the simulation results where potentially different signal to noise levels were not modeled. Thus, we normalized our different bistatic measurements so that they have the same energy. This, however, might not be the case in practice as different bistatic receivers might capture different levels of returned energy

even in the case of an ideal spherical target. As a result, both the probability of detection and resolution might be affected. This issue will be studied in future work.

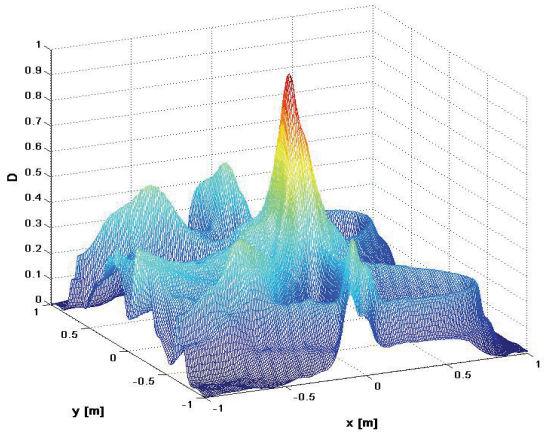

Figure 10. Normalized multistatic data cube (first configuration)

Let us comment on the shape of the normalized multistatic data cube shown in Figure 10. First we observe the ability of the multistatic system to localize the target in space as was already suggested in our simulations (see Figure 2). In our comparisons with simulations we are primarily interested in the main lobe 3-dB area. For the measured system configuration it equals **0.0712 m^2** as can be computed form the date cube. One can also notice certain patterns outside the main lobe that we do not see in our previous simulations (see, for example, Figure 2). This is due to the relative size of the interrogation area. While in the case of our simulations, distances among the transmitter, receivers and the target were much greater (~ 10 km) than the size of the interrogation area (100m x 100m), in the case of measurements they were at the same order of magnitude.

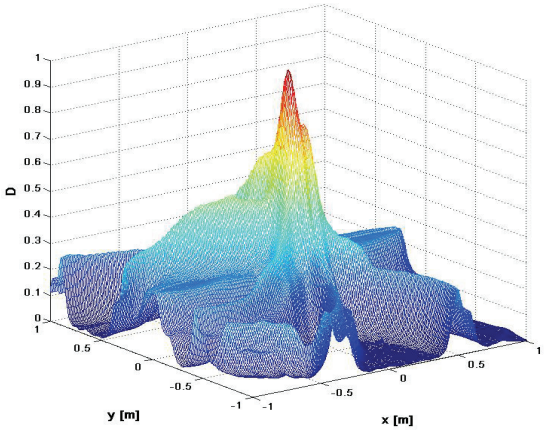

Figure 11. Normalized multistatic data cube (second configuration)

Next we changed the multistatic system configuration and positioned the four bistatic receivers at $\phi_1 = \pi/12$, $\phi_2 = 19\pi/12$, $\phi_3 = 13\pi/12$ and $\phi_4 = 7\pi/12$. This is the same configuration as the one in Figure 4 for the transmitter located at $\alpha = \pi/12$. The corresponding normalized multistatic data cube is shown in Figure 11. This time the measured main lobe 3-dB area equals **0.0796 m^2**. Thus, we experienced degradation in resolution which is consistent with our simulation results (see Figure 5).

VI. Conclusions

In this paper we presented multistatic measurements obtained in a controlled laboratory environment. Different multistatic system geometries were considered. We were able to verify the theoretical findings regarding the sensor placement that were based on the multistatic ambiguity function. The measured main lobe 3-dB area results closely match the results obtained in simulations (speaking in relative terms since the waveform used and relative distances were different). Future work is needed to investigate in measurements the role of waveform selection and weighting of different receivers play in multistatic radar systems and compare results with the theoretical findings.

The views expressed in this article are those of the authors and do not reflect the official policy or position of the United States and Royal Australian Air Forces, the respective Departments of Defense, or the U.S. and Australian Governments.

References

[1] T. Tsao, M. Slamani, P.K. Varshney, D.D. Weiner, and H. Schwarzlander, "Ambiguity Function for a Bistatic Radar," *IEEE Transactions on Aerospace and Electronic Systems*, Vol. 33, No. 3, July 1997.

[2] D.D. Weiner, M.C. Wicks, and G.T. Capraro, "Waveform Diversity and Sensors as Robots in Advanced Military Systems," *1st International Waveform Diversity and Design Conference*, Edinburgh, UK, November 2004.

[3] I. Bradaric, G.T. Capraro, D.D. Weiner, and M.C. Wicks, "Multistatic Radar Systems Signal Processing," *IEEE Conference on Radar*, Verona, New York, USA, April, 2006.

[4] I. Bradaric, G.T. Capraro and P. Zulch, "Signal Processing and Waveform Selection Strategies in Multistatic Radar Systems," *International Waveform Diversity and Design Conference*, Pisa, Italy, June 2007, invited paper.

[5] I. Bradaric, G.T. Capraro, and M. C. Wicks, "Waveform Diversity for Different Multistatic Radar Configurations," *Asilomar Conference on Signals, Systems, and Computers*, November 2007.

[6] I. Bradaric, G.T. Capraro, and M.C. Wicks, "Sensor Placement for Improved Target Resolution in Distributed Radar Systems," *IEEE Radar Conference*, Rome, Italy, May 2008.

[7] Lab-Volt Ltd, *Principles of RADAR Systems*, 2nd ed. Quebec, Canada: Lab-Volt Ltd, September 1990.

[8] S. Brady and M. Saville, "Scaling Radar Measurements for Advanced Algorithms," *IEEE International Radar Conference*, Washington DC, USA, May 2010.